Global NEST Journal, **28** (8), 08616
Available online: 16/09/2026

7

Electrocatalytic Nitrite Reduction by an Iron-Based Sandwich Polyoxometalate: A Preliminary Study

Chaima Krikeb[1]*, Robila Belghiche[1], Valérie Marvaud[2], Safia Alleg[3], and Geoffrey Gontard[2]

[1]Laboratory of Inorganic Materials Chemistry, Department of Chemistry, Faculty of Science, University of Annaba, B. P. 12, 23000 Annaba, Algeria,
[2] Institut Parisien de Chimie Moléculaire (IPCM), UMR 8232, Sorbonne University, 4 Place Jussieu, 75252 Paris Cedex 05, France
[3]Laboratory of Magnetism and Spectroscopy of Solids, Department of Physics, Faculty of Science, University Badji Mokhtar of Annaba, B. P. 12, 23000 Annaba, Algeria

*Correspondence e-mail: chaima.krikeb@univ-annaba.dz

Abstract

A sandwich-type polyoxometalate, $K_4Na_7[(\alpha\text{-}SiFe_3W_9(OH)_3O_{34})_2(OH)_3]\cdot 56H_2O$ (POM-Fe), was synthesized and comprehensively characterized and its electrocatalytic activity toward nitrite reduction was investigated. The chemical composition of the compound was confirmed by energy-dispersive X-ray fluorescence (EDXRF), energy-dispersive X-ray spectroscopy (EDX), and thermogravimetric analysis (TGA), while its structural and spectroscopic properties were investigated by powder X-ray diffraction, IR, and UV–Vis spectroscopy. Single-crystal analysis further confirmed the consistency of POM-Fe with the previously reported sandwich-type polyoxometalate structure. Magnetic measurements revealed paramagnetic behavior, with a saturation magnetization of 0.0646 emu/g. The electrochemical behavior of POM-Fe toward nitrite reduction was evaluated by cyclic voltammetry at pH 4.8 and 3.0, with a markedly enhanced electrocatalytic response observed at pH 4.8. The electrochemical response in the presence of nitrite demonstrated the catalytic activity of POM-Fe toward nitrite reduction under the investigated conditions. Qualitative detection of ammonia using the Nessler method further suggested the formation of ammonia as a reduction product. These results demonstrate the potential of POM-Fe as an iron-based polyoxometalate electrocatalyst for nitrite reduction and highlight its possible relevance to electrochemical approaches for environmental remediation.

Keywords: Electroreduction, nitrite, polyoxometallates, silicotungstates, cyclic voltammetry.

OPEN ACCESS

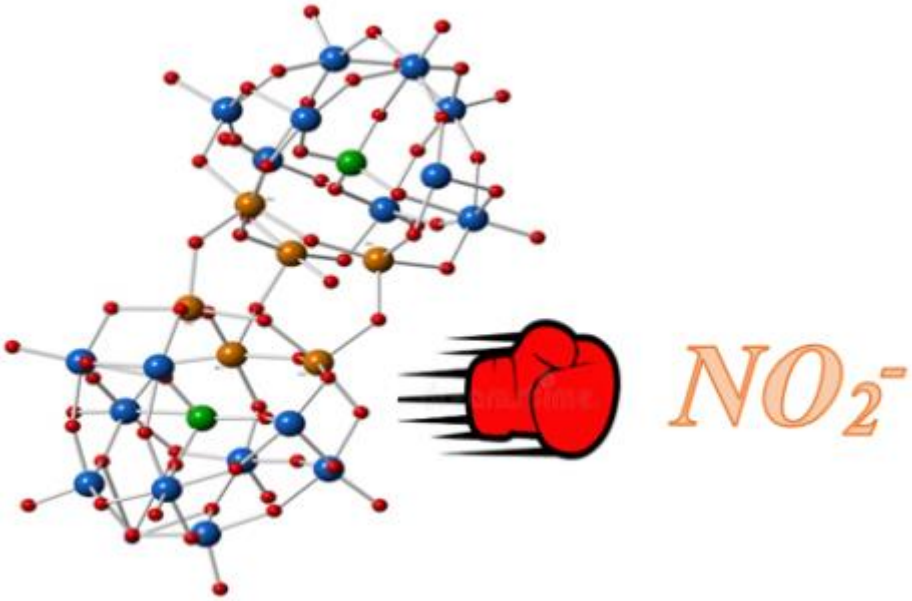
Received: 05/05/2024,

Accepted: 09/09/2026,

Available online: 16/09/2026

Copyright: © 2026 The Author(s). Published in Global NEST Journal. This article is licensed under the terms and conditions of the Creative Commons Attribution 4.0 International license (CC BY 4.0).

Graphical abstract



1. Introduction

Nitrite (NO_2^-) is a harmful nitrogenous contaminant frequently found in groundwater, wastewater, and various industrial effluents. Its accumulation in natural environments can trigger severe ecological disturbances, including eutrophication and a marked decline in water quality. From a human health perspective, nitrite is particularly hazardous, as it can lead to the formation of carcinogenic N-nitroso compounds and induce methemoglobinemia, especially in infants and pregnant women (Ward *et al.* 2018; Fewtrell *et al.* 2004; Picetti *et al.* 2022). These associated risks have stimulated increasing interest in efficient strategies for nitrite removal or conversion.

Among the available remediation approaches, the electrocatalytic reduction of nitrite (NO_2RR) has emerged as a cost-effective and environmentally benign alternative. In contrast to thermal or biological treatments, electrochemical nitrite reduction operates under mild conditions, requiring neither elevated temperatures nor high-pressure systems, thus offering a controllable and energy-efficient route for pollutant transformation.

Within this context, polyoxometalates (POMs) have attracted considerable attention. POMs are discrete anionic metal–oxide clusters composed mainly of early transition metals (W, Mo, V) interconnected through oxygen atoms. Their rich redox properties, structural versatility, and high stability make them valuable molecular catalysts for applications in electrocatalysis, photochemistry, and molecular electronics (Gusmão *et al.* 2022; Bao *et al.* 2025; Li *et al.* 2024; Cherevan *et al.* 2020; Wang *et al.* 2025). Their ability to incorporate multiple redox-active metal centers enables POMs to mediate complex multi-electron processes with high selectivity.

Several studies have reported the use of polyoxometalate (POM)-based systems for the electrocatalytic reduction of nitrite in homogeneous solution, where the catalyst operates as a dissolved molecular species rather than a surface-confined material, demonstrating promising catalytic performance. For instance, Zhou *et al.* (2022) investigated the electrocatalytic reduction of HNO_2/NO_2^- at pH 2 and 5 using reduced Keggin-type POMs, namely $[PW_{12}O_{40}]^{3-}$, $[SiW_{12}O_{40}]^{4-}$, and $[BW_{12}O_{40}]^{5-}$. Ruhlmann *et al.* (2004) demonstrated that the anion $K_{28}H_8[P_2W_{15}Ti_3O_{60}{\cdot}5]_4$ exhibits electrocatalytic activity toward HNO_2 reduction at pH 3.5. Zonoz *et al.* (2016) explored nitrite reduction using $Cd_2Zn_2P_4W_{30}$ at pH 4.7, selected to minimize complications related to HNO_2 disproportionation ; this catalyst displayed an efficiency of 36.6 %. Additionally, Ruhlmann *et al.* (2002); (2007) evaluated the catalytic efficiency (CAT) of $NaMn_3P_4W_{30}$, $NaCo_3P_4W_{30}$, and $Co_4P_4W_{30}$ across a range of pH values. For example, $NaCo_3P_4W_{30}$ exhibits catalytic efficiencies of 300 %, 220 %, 88 %, and 28 % at pH 0.59, 1.77, 2.52, and 3.00, respectively. Furthermore, $Cu_4P_4W_{30}$ has shown significant catalytic activity for nitrite reduction at pH 5, particularly at high NO_2^- concentrations, a behavior attributed to the specific properties of its transition-metal centers (Keita *et al.* 2003). Li *et al.* (2005) synthesized the germanium (IV) based compound $[Fe_6(OH)_3(A\text{-}\alpha\text{-}GeW_9O_{34}(OH)_3)_2]^{11-}$, which also demonstrated notable catalytic activity for nitrite reduction at pH 3. Collectively, these findings highlight POMs as one of the most promising families of catalysts for electrocatalytic nitrite reduction.

The development of controlled synthetic routes for complex iron-substituted polyoxometalates remains a significant challenge in POM chemistry. In particular, iron-rich sandwich-type polyoxometalates remain scarcely explored in terms of reproducible synthesis and their

electrocatalytic behavior toward nitrite reduction. In this context, $K_4Na_7[(\alpha\text{-}SiFe_3W_9(OH)_3O_{34})_2(OH)_3]$, previously reported by Anderson *et al.* (2004) and featuring a Fe_6 sandwich architecture, represents an attractive platform for investigating the electrochemical reactivity of multi-iron POM systems.

Herein, we report a buffered synthetic strategy at pH 4.8 that enables the reproducible preparation of $K_4Na_7[(\alpha\text{-}SiFe_3W_9(OH)_3O_{34})_2(OH)_3]$. Spectroscopic characterization, together with powder X-ray diffraction and single-crystal X-ray analysis, confirmed the formation and structure of the synthesized compound. The controlled buffered conditions provide a reproducible preparation route and constitute an important aspect of the present work.

Furthermore, the electrochemical behavior of this iron-rich sandwich-type polyoxometalate toward nitrite reduction was investigated in homogeneous solution. Cyclic voltammetry revealed enhanced electrocatalytic activity in the presence of nitrite, particularly at pH 4.8. Qualitative ammonia detection using the Nessler method provided evidence for ammonia formation during nitrite reduction. The novelty of the present work lies in combining a reproducible buffered synthesis of the Fe_6 sandwich-type polyoxometalate at pH 4.8 with its first electrocatalytic investigation toward nitrite reduction in homogeneous solution. These findings highlight the potential of multi-iron polyoxometalate architectures for the electrocatalytic reduction of nitrite.

2. Experimental

2.1. *Materials*

All chemicals were purchased from commercial sources and used without further purification. The crystallographic data for the compound were collected at 200K from single crystals mounted on a loop fiber using a Bruker Kappa APEX-II CCD diffractometer using a graphite-monochromated Mo-Kα radiation (λ=0.71073Å). Powder X-ray diffraction (PXRD) patterns were recorded using an Empyrean Panalytical diffractometer equipped with a PIXCEL 1D detector (Amedipix3 collaboration).

The IR spectra were recorded between 4000 and 500 cm-1 using a SHIMADZU IRSpirit spectrometer. The cyclic voltammograms were obtained at room temperature using a BioLogic SP-300 potentiostat, in a three-electrode cell with a Pt plate auxiliary electrode, a glassy carbon working electrode (GCE) of 7 mm^2 surface area and a saturated calomel reference electrode (SCE). The solutions are degassed with pure argon for at least 30 minutes. UV-VIS spectra were recorded in aqueous solution from 200 to 800 nm using a JENWAY 7315 UV-VIS spectrometer. The thermal analysis was investigated under an N2 atmosphere from room temperature to 800 °C on SDT Q600 simultaneous TGA analyzer. The SEM instrument used was Quanta 250, EDX Ametek EDAX model: octanepro-A. EDXRF: S2PUMA-BRUKER. The magnetic measurements were carried out with a Bull M 2000 SIIS hysteresis meter at ambient temperature.

2.2. *Synthesis*

2.2.1. $Na_{10}[\alpha\text{-}SiW_9O_{34}].23H_2O$

$Na_{10}[\alpha\text{-}SiW_9O_{34}]$ is the tri-lacunary Keggin polyoxometallate, and was synthesized from sodium tungstate and sodium metasilicate according to the procedure described in the literature (Tézé, Hervé. 1990).

2.2.2. $K_4Na_7[\{\alpha\text{-}SiFe_3W_9(OH)_3O_{34}\}_2(OH)_3].56H_2O$

$Na_{10}[\alpha\text{-}SiW_9O_{34}].23H_2O$ (3.00 g, 1.0449 mmol) was dissolved in 150 ml of buffer solution pH = 4.8 NaOAc/HOAc. $FeCl_3$ (0.5084g, 3.1347 mmol) was slowly added to the solution with slow stirring. Then, the mixture was heated at 80 °C for 1 h. After cooling the solution to room temperature, 3g of solid KCl was added to the solution with slow stirring for 30 minutes, a green precipitate obtained was recovered by filtration with yield of 80 %, crystals were obtained in a 4.8 buffer solution after 2 days at room temperature. IR (1200-500cm^{-1}): ύ = 1123.33(w), 995.09 (w), 949.77(m), 896.741(s), 779.10(s), 733.78 (s), 521.65(w, b), 475.37(w). Elemental analysis, calculated: Na: 2,95; K: 6,20; Fe: 3,52; W: 56,17; Si: 0,95. Experimental (EDXRF): Na: 2,52; K: 5,66; Fe: 2,88; W: 55,87; Si: 0,91.

3. Results and discussion

3.1. *IR Spectroscopy*

The IR spectrum of $\alpha\text{-}Na_{10}[SiW_9O_{34}]$ shows vibrational bands close to those found in the literature (Tézé, Hervé. 1990), between 2000 and 400 cm^{-1} which is the fingerprint region of the infrared spectra of POMs. The IR spectrum of POM-Fe exhibits all the characteristic vibrational bands of the sandwich anion (Anderson *et al.* 2004), as shown in **Figure 1**. The band located at 1123.33 cm^{-1} is assigned to the asymmetric stretching vibration ν_{as}(Si–Oa), while the bands at 995.09 cm^{-1}, 949.77 cm^{-1}, 896.74 cm^{-1}, 779.10 cm^{-1}, 733.78 cm^{-1}, 521.65 cm^{-1}, and 475.37 cm^{-1} correspond respectively to the asymmetric stretching vibrations ν_{as}(W–Ot), ν_{as}(W–Ob), and ν_{as}(W–Oc). Compared with the precursor $\alpha\text{-}Na_{10}[SiW_9O_{34}]$, the observed spectral modifications suggest the formation of a sandwich-type polyoxometalate structure consistent with the compound previously reported in the literature.

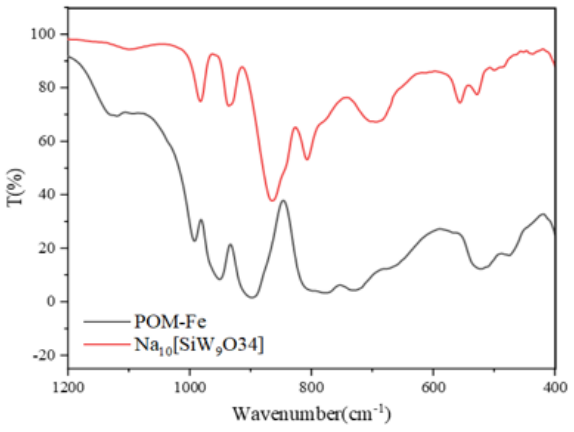


Figure 1. IR spectra of the polyoxometallates $\alpha\text{-}Na_{10}[SiW_9O_{34}]$ and POM-Fe.

3.2. *UV-Visible Spectroscopy*

Figure 2 shows the UV–Vis absorption spectrum of POM-Fe. The spectrum exhibits an absorption band in the visible

region, with a characteristic band centered at 436 nm attributed to Fe(III) d–d transitions. This observation is consistent with the incorporation of iron within the polyoxometalate framework and agrees with previously reported data for similar sandwich-type compounds described by Travis Anderson. The absorbance measured for the 2 mM solution (A = 0.30) corresponds to an experimental molar extinction coefficient of ε ≈ 150 $M^{-1}·cm^{-1}$, which is close to the literature value reported for a 4 mM solution (ε = 146 $M^{-1}·cm^{-1}$).

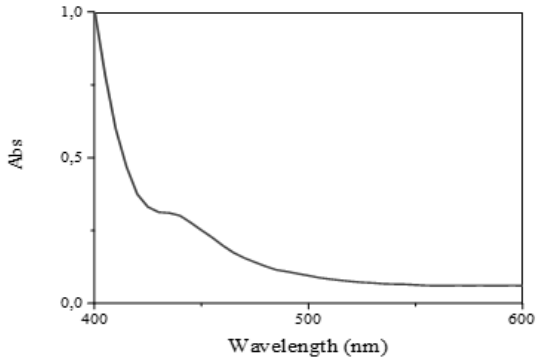


Figure 2. UV-Visible spectra of a 2.10^{-3} M of POM-Fe.

3.3. *Scanning electron microscopy (SEM) and X-ray fluorescence spectrometry (EDXRF)*

The morphology of the POM-Fe compound was investigated by scanning electron microscopy (SEM), as shown in Figure 3. The SEM image recorded at a 50 µm scale reveals a relatively homogeneous surface composed of hexagonal-like entities. This morphology is consistent with the formation of an organized polyoxometalate-based material and suggests a relatively uniform distribution of the observed structures.

Energy-dispersive X-ray spectroscopy (EDS) analysis confirmed the presence of the main constituent elements of the synthesized compound, as shown in **Figure 4**, supporting the expected chemical composition. The bulk elemental composition was further examined by X-ray fluorescence (XRF), and the corresponding results are summarized in **Table 1**. The XRF results are consistent with the proposed stoichiometry of $K_4Na_7[(\alpha\text{-}SiFe_3W_9(OH)_3O_{34})_2(OH)_3]$.

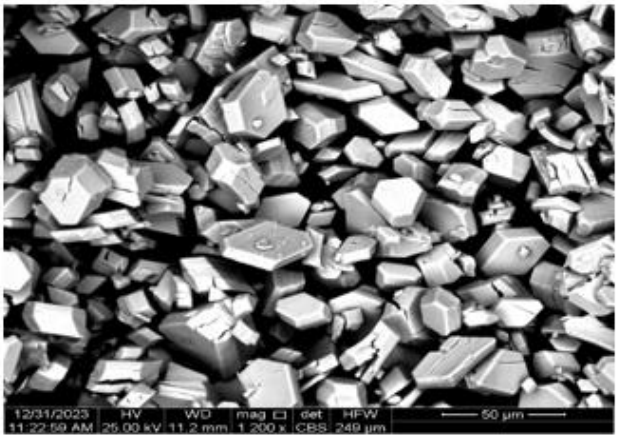


Figure 3. SEM images of POM-Fe.

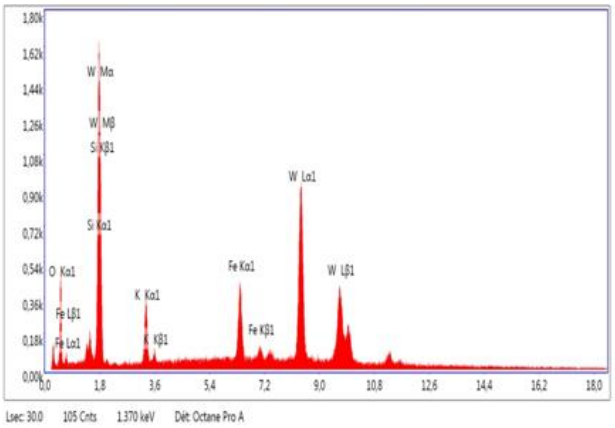


Figure 4. EDX spectrum of POM-Fe.

Table 1. EDXRF results for POM-Fe.

Element	%Theoretical mass POM-Fe	%experimental mass (EDXFR)
Si	0.95	0.91
K	6.20	5.66
Na	2.95	2.52
W	56.17	55.87
Fe	3.52	2.88

Table 2. Electrochemical data of POMs.

Compounds	E_{pc}^{W} (V)	E_{pa}^{W} (V)	$E_{1/2}^{W}$ (V)	ΔE_p^{W} (V)	E_{pc}^{Fe} (V)	E_{pa}^{Fe} (V)	$E_{1/2}^{Fe}$ (V)	ΔE_p^{Fe} (V)
$Na_{10}[SiW_9O_{34}]$	-0,837	-0,741	-0,789	-0,096	/	/	/	/
POM-Fe	-0,843	-0,736	-0,790	0,107	-0,346	0,041	-0,152	0,387

E_{pc}: Cathodic reduction potential; E_{pa} : Anodic oxidation potential; $E_{1/2}$: Half-wave potential $E_{1/2} = (E_{pc} + E_{pa})/2$; $\Delta Ep = Epa - Epc$.

3.4. *Single-Crystal and Powder X-ray Diffraction Analysis*

The crystal structure of the synthesized compound was examined by single-crystal X-ray diffraction using several individual crystals. The obtained lattice parameters were found to be in good agreement with those reported for the iron-substituted sandwich-type polyoxometalate described by Anderson *et al.* (2004), supporting the assignment of the synthesized compound to the same lattice system. A representation of the corresponding unit cell is presented in **Figure 5**. In parallel, the powder X-ray diffraction pattern was recorded, analyzed using HighScore software, and compared with the simulated diffractogram generated from the crystallographic data previously reported by Anderson *et al.* (COD No. 4312017). The diffraction peak positions (2θ) are consistent with those of

the previously reported iron-substituted sandwich-type polyoxometalate, suggesting preservation of the main structural framework (**Figure 6**). Slight variations in relative intensities may arise from experimental factors such as preferred crystallite orientation and particle size distribution. Rietveld refinement provided satisfactory agreement factors (R_{Bragg} = 7.22%, $R_{profile}$ = 7.47%, χ^2 = 1.7), supporting the structural similarity between the synthesized compound and the iron-substituted sandwich-type polyoxometalate previously described by Anderson *et al.*

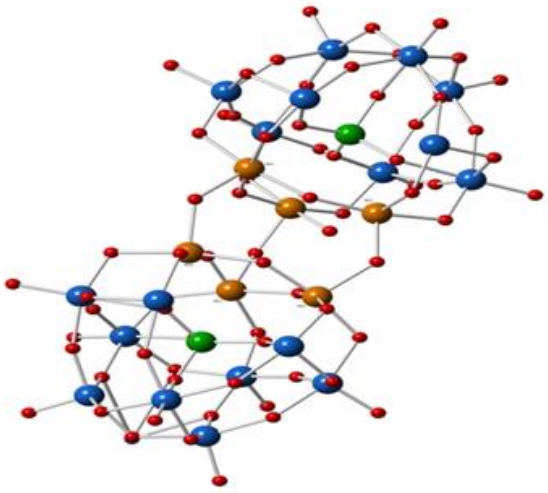


Figure 5. Ball and stick representation of [{α-$SiFe_3W_9(OH)_3O_{34}$}$_2$$(OH)_3$]$^{-11}$.The color code is as follow : iron (orange), tungsten (bleu), silicon (green), oxygen (red).

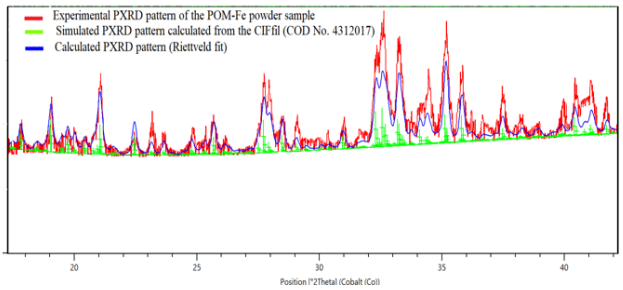


Figure 6. Experimental powder X-ray diffraction (PXRD) pattern of the POM–Fe powder compared with the simulated pattern calculated from the CIF file (COD No. 4312017) and the refined pattern obtained from Rietveld analysis.

3.5. *Thermal and VSM analysis*

Thermogravimetric analysis (TGA) of the compound $K_4Na_7[(\alpha\text{-}SiFe_3W_9(OH)_3O_{34})_2(OH)_3]\cdot nH_2O$ reveals a multistep weight-loss profile typical of hydrated polyoxometalates (**Figure 7**). The first weight loss of approximately 16% observed below 200 °C is attributed to the removal of crystallization water molecules weakly bound within the crystal lattice through electrostatic interactions and hydrogen bonding with the alkali metal cations. Based on this mass loss and the calculated molar mass of the anhydrous framework (5258 g·mol^{-1}), the hydration number was estimated to be approximately 56 water molecules per formula unit. A second, broader weight loss occurring between 600 and 850 °C is associated with the dehydroxylation of OH groups and the thermal decomposition of the polyoxotungstate framework. The observed high degree of hydration is consistent with the large size of the cluster and its high negative charge density.

The magnetic behavior of POM-Fe was investigated using a vibrating sample magnetometer (VSM) at 295 K. The hysteresis curve of this compound (**Figure 8**) shows low coercivity and weak remanence, with a saturation magnetization of 0.0646 emu/g, consistent with a predominantly paramagnetic behavior. The low remanence (Mr) suggests a soft magnetic response. The molar magnetic susceptibility was calculated and used to estimate the effective magnetic moment, giving μ_{eff} = 8.6 μ_B/mole.

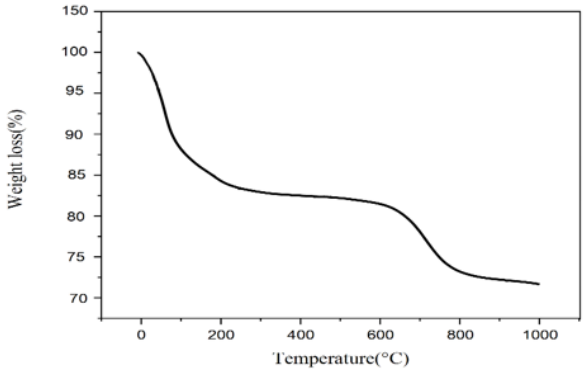


Figure 7. TGA curve of POM-Fe.

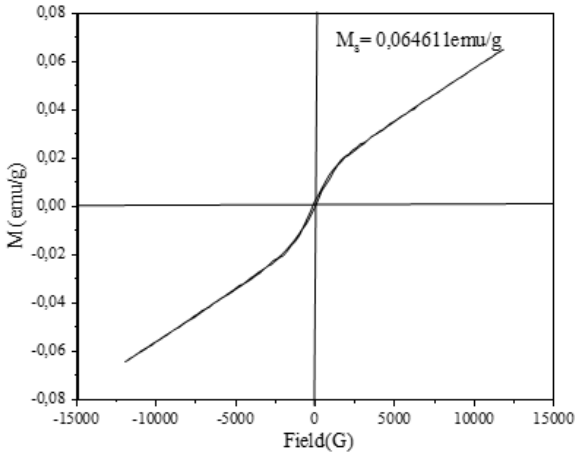


Figure 8. VSM curve of POM-Fe.

3.6. *Electrochemical study*

The electrochemical behavior was studied in two different media at pH 4.8 (0.5 M CH_3COONa + CH_3COOH) and pH 3 (0.2 M Na_2SO_4 + H_2SO_4). Each electrochemical experiment, performed using a BioLogic SP-300 potentiostat, was repeated several times to ensure good reproducibility.

The cyclic voltammogram of POM-Fe at a concentration of 10^{-4} M was recorded at pH 4.8 with a scan rate of 10 mV s^{-1} (**Figure 9a**), is shown in red and exhibits two reduction peaks. The first peak, at −0.346 V vs SCE, is attributed to the reduction of Fe^{3+} ions (Bi *et al.* 2005; Anderson *et al.* 2005), in agreement with the Epc value of −0.406 V vs SCE reported for polyoxometalates $[Fe_4(H_2O)_{10}(\beta\text{-}AsW_9O_{33})_2]^{6-}$ under similar conditions (Ni *et al.* 2011). The second peak, at −0.843 V vs SCE, corresponds to the reduction of W^{6+} ions (Bi *et al.* 2005). This interpretation is confirmed by

comparing the voltammograms of POM-Fe with those of its precursor $Na_{10}[SiW_9O_{34}]$, where POM-Fe exhibits a peak at −0.843 V vs SCE, compared to −0.837 V vs SCE for $Na_{10}[SiW_9O_{34}]$ under identical conditions (**Figure 9a**). The slight shift in the tungsten reduction peaks between the precursor and POM-Fe is likely due to the incorporation of iron centers between two trilacunary Keggin-type $Na_{10}[SiW_9O_{34}]$ units. Notably, tungsten centers in the precursor are reduced more readily than in POM-Fe. This behavior can be attributed to the lower overall negative charge of $Na_{10}[SiW_9O_{34}]$, which facilitates electron uptake, whereas the higher negative charge of POM-Fe makes the reduction process more difficult. As generally observed for polyoxometalates, reduction becomes increasingly hindered as the overall charge of the anion becomes more negative.

Under identical experimental conditions, the reduction of Fe^{3+} in $FeCl_3$ occurs at a positive potential around 0.183 V vs SCE compared to the reduction of Fe^{3+} in POM-Fe at −0.346 V vs SCE, as shown in **Figure 9b**. This shift toward more negative potentials in POM-Fe indicates that the reduction of iron is less favorable, which can be attributed to the strong coordination of Fe centers within the polyoxometalate framework. In contrast, in $FeCl_3$, iron ions are more freely accessible in solution, facilitating electron transfer and thus reduction at positive potential.

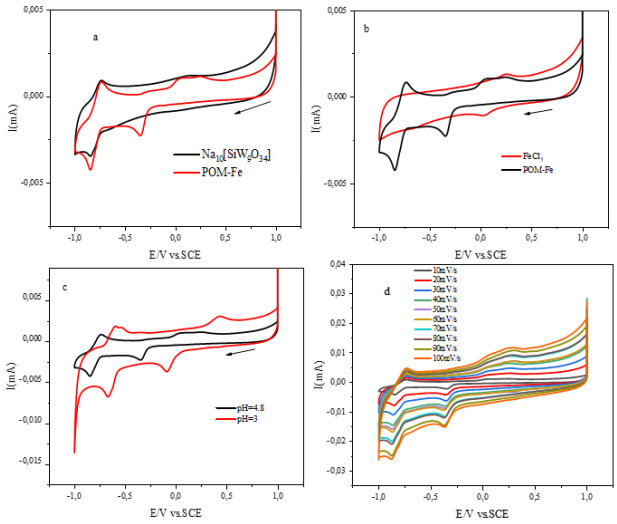


Figure 9. (a) CV of POM-Fe and $Na_{10}[SiW_9O_{34}]$. (b) CV of POM-Fe and $FeCl_3$. (c) Comparison of CV of POM-Fe at pH 3 and 4.8. C (POM-fe)=1×10^{-4}M, $C_{Na10[SiW9O34]}$ =1×10^{-4}M and $C_{(FeCl3)}$ =1×10^{-4}M , scan rate 10 mV.s^{-1} (d) CV of POM-Fe recorded at scan rates varying from 10 to100 mV.s^{-1}.

The electrochemical behavior of POMs is pH dependent (Zhu *et al.* 2012). **Figure 9c** shows the evolution of the Fe and the W peaks as the pH varies from 4.8 to 3. There is a shift of the peaks towards less negative potentials with increasing supporting electrolyte acidity. In **Figure 9d**, cyclic voltammograms were recorded at different scan rates ranging from 10 to 100 mV s^{-1}. The voltammograms were superimposed using Origin software. It is observed that increasing the scan rate leads to an increase in both oxidation and reduction peak currents, while the shape of the redox couple is maintained.

Figure 10 was used in order to investigate the mechanism and kinetics of the electrochemical processes. Both anodic and cathodic peak currents increase linearly with the square root of the scan rate (Ip ∝ υ$^{1/2}$), indicating that the electron-transfer process is predominantly diffusion-controlled. In addition, the anodic and cathodic peak potentials remain nearly independent of the scan rate, as evidenced by the linear evolution of Ep versus log v with an approximately zero slope. This behavior is characteristic of a fast and quasi-reversible electron-transfer system, in which the kinetics are sufficiently rapid to maintain equilibrium at the electrode surface (Li *et al.* 2020).

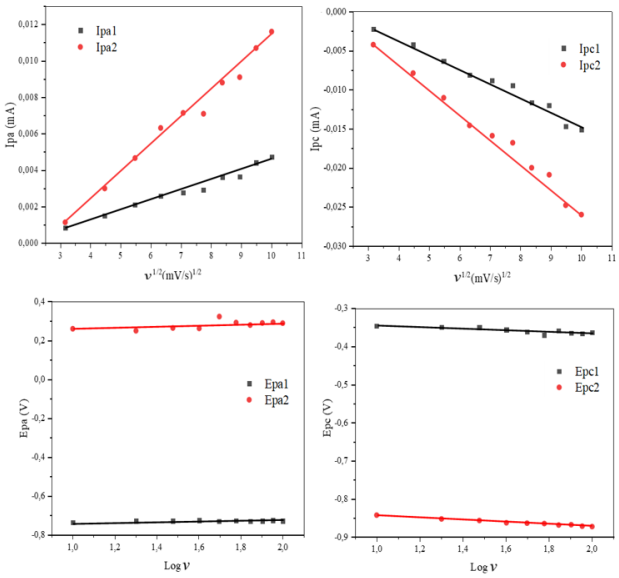


Figure 10. Relationship of Ipc and Ipa vs square root of scan rate (υ$^{1/2}$) and log υ at 25ºC.

3.7. *Electrocatalytic reduction of nitrite ions*

The reduction of NO_x ions is an electrochemical conversion method that transforms these abundant nitrogen species into value-added chemicals such as hydroxylamine (NH_2OH), nitrous oxide (N_2O), and ammonium (NH_4^+).

The interest in NO_x reduction is primarily driven by environmental concerns. In particular, nitrite (NO_2^-) and nitrate (NO_3^-) ions pose significant challenges during high-temperature treatment of nuclear waste, as their presence can lead to the emission of toxic gases (Genders *et al.* 1996 ; Li *et al.* 1988). Nitrite contamination is also a major environmental concern due to its high solubility and persistence in aquatic systems. Elevated nitrite concentrations in water can contribute to eutrophication and may pose serious risks to human health through the formation of carcinogenic N-nitroso compounds. Consequently, the development of efficient electrocatalytic systems capable of converting nitrite into less harmful or value-added products under mild conditions represents an important challenge in environmental remediation and sustainable chemistry.

This context highlights the need for efficient catalytic systems capable of promoting the controlled electrochemical reduction of NO_x under mild conditions. In this regard, polyoxometalates (POMs) have emerged as promising catalysts due to their multivalent redox

properties and their ability to store and transfer multiple electrons, making them particularly suitable for electrocatalytic reduction processes. Notably, the first investigations of POMs in the homogeneous electrocatalytic reduction of NO_x were reported by Nadjo *et al.* (2001). In these systems, the metal center, particularly iron in the present case, serves as the active site within the molecular framework, facilitating nitrite activation through coordination and the formation of metal–nitrosyl (M–NO) intermediates, which represent key reactive species prior to multi-electron reduction steps (Mitchell *et al.* 2025). The final conversion to ammonia occurs at more negative potentials, where the required electrons are supplied by the tungsten framework of the POM, which functions as a multi-electron reservoir.

All electrochemical measurements were performed using freshly prepared solutions, which were degassed with argon for 30 min to remove dissolved oxygen and prevent interference from oxygen reduction. Prior to each electrochemical experiment, the glassy carbon electrode (GCE, 7 mm^2 surface area) was mechanically polished with an alumina slurry on a polishing cloth until a mirror-like surface was achieved. The electrode was then thoroughly rinsed with deionized water and successively sonicated in ethanol and ultrapure water to remove any residual particles. This polishing procedure was repeated before every measurement to ensure high reproducibility. After drying under ambient conditions, the cleaned GCE was directly employed as the working electrode for cyclic voltammetry experiments in the electrolyte solution. The observed electrocatalytic activity therefore arises from a homogeneous catalytic process occurring in solution. In this system, POM–Fe acts as a soluble redox mediator, promoting electron transfer between the electrode and nitrite species.

McCormac *et al.* (1997) reported that at pH 2.00, the nitrite concentration decreases significantly due to the formation of its conjugate acid, nitrous acid (HNO_2), which is both chemically unstable and volatile. This behavior can be described by the following equations:

$$HNO2 \leftrightarrow H+ + NO2\text{-}pKa = 3,3 \text{ at } 18°C \quad (1)$$

$$3HNO2 \leftrightarrow HNO3 + 2NO + H2O \quad (2)$$

Although the kinetics of nitrite disproportionation are relatively slow, it is essential to maintain the solution pH above 4.0 to ensure that nitrite (NO_2^-) remains the predominant nitrogen species. Accordingly, the electrocatalytic reduction of nitrite was investigated at pH 4.8, where NO_2^- exhibits sufficient chemical stability. At this pH, nitrite is the dominant species, whereas in more acidic media, HNO_2 predominates.

Cyclic voltammetry measurements were carried out in acetate buffer at pH 4.8 containing POM–Fe at a fixed concentration of 1×10^{-4} M. A baseline voltammogram was first recorded in the absence of nitrite (**Figure 11a**, black curve). Subsequently, fresh solutions were prepared for each nitrite concentration, and $NaNO_2$ was added at increasing concentrations. For clarity, the dimensionless parameter γ was defined as the ratio of nitrite concentration to catalyst concentration ($\gamma = C_{(NO_2^-)}/C_{(POM-Fe)}$) (Belhouari *et al.* 1998; Keita *et al.* 2003). Accordingly, γ = 0 corresponds to the absence of nitrite, while γ = 10, 30, and 60 correspond to $NaNO_2$ concentrations of 1×10^{-3}, 3×10^{-3}, and 6×10^{-3} M, respectively.

As shown in **Figure 11**, the addition of nitrite induces a pronounced increase in the cathodic current, which increases progressively with nitrite concentratio, starting at potentials preceding the tungsten reduction. In the absence of nitrite, the reduction of tungsten occurs at −0.84 V vs SCE. Upon addition of nitrite, a catalytic current arises at less negative potentials (−0.65 to −0.70 V vs SCE), indicating that nitrite reduction proceeds via electron transfer from the reduced tungsten centers within the POM–Fe framework. This shift toward less negative potentials, together with the progressive loss of reversibility of the anodic wave associated with tungsten centers in POM–Fe. In this process, the reduced tungsten species act as electron mediators, rapidly transferring electrons to nitrite, thereby facilitating the overall reduction and decreasing the required overpotential. These results highlight the efficient electrocatalytic performance of POM–Fe, whereas no significant reduction of nitrite is observed in the absence of the catalyst (**Figure 12**).

The current enhancement can be quantified using the catalytic efficiency (CAT), defined as (belhouari *et al.* 1998; Keita *et al.* 2003) :

$$\mathrm{CAT}(\%) = 100 \times \frac{I_{(\mathrm{POM}+\mathrm{NO_2^-})} - I_{(\mathrm{POM})}}{I_{(\mathrm{POM})}}$$

Where represents the reduction current of POM–Fe in the presence of nitrite, and corresponds to that of POM–Fe alone. In the present experiments, CAT values at pH 4.8 increase significantly with γ, rising from 375.25% to 1577.45% as γ increases from 10 to 60. The catalytic efficiency reaches 1577.45% at pH 4.8, while a lower value of 637.24% is obtained at pH 3.0. This decrease under more acidic conditions may be attributed to the predominance of HNO_2, a less stable species prone to disproportionation and partial volatilization (Bi *et al.* 2005).

To further evaluate the catalytic performance, the present results were compared with other tungsten-based polyoxometalates reported in the literature. Relatively lower catalytic efficiencies were reported for $Cd_4P_4W_{30}$, $Cd_2Zn_2P_4W_{30}$, and $Zn_4P_4W_{30}$, with maximum CAT values of 14.2%, 36.6%, and 174.7% at pH ≈ 4.7, respectively (Zonoz *et al.* 2016). In addition, for the copper-based polyoxometalate $[Cu_5(OH)_4(H_2O)_2(\alpha\text{-}SiW_9O_{33})]^{10-}$, catalytic efficiencies for nitrate reduction were reported, with CAT values ranging from 618% to 1393% as γ increased from 10 to 30 in a pH 5 acetate buffer medium (Nellutla *et al.* 2005).

In comparison, the present POM–Fe system shows higher catalytic efficiencies for nitrite reduction under similar pH conditions (pH 4.8). This comparison suggests that the POM–Fe catalyst exhibits promising electrocatalytic activity toward nitrite conversion.

Two successive chronoamperometric electrolyses were carried out in a 30 mL acetate buffer solution (acetic

acid/sodium acetate, 0.50 M) at pH 4.8, containing POM–Fe (1 × 10^{-4} M) and NO_2^- (6 × 10^{-3} M). The same electrochemical cell and working electrode described above were used. Prior to electrolysis, the solution was purged with argon, and magnetic stirring was maintained throughout each electrolysis step. The applied potentials were selected based on the voltammetric behavior of POM–Fe, where the reduction waves of the iron and tungsten centers occur at −0.346 V and −0.843 V vs SCE, respectively. Accordingly, the first electrolysis was performed at −0.40 V vs SCE, slightly more negative than the iron-centered reduction wave, while the second was conducted at −0.90 V vs SCE, more negative than the tungsten-centered reduction region. Each electrolysis step was maintained for 30 min, and the two successive electrolyses were performed in the same solution without replacing the electrolyte.

Table 3. Catalytic efficiencies at pH 4.8 .

[$NaNO_2$] (M)	E (V vs SCE)	CAT %
10^{-3}	-0.663	375.247
3×10^{-3}	-0,659	1437.255
6×10^{-3}	-0.659	1577.45

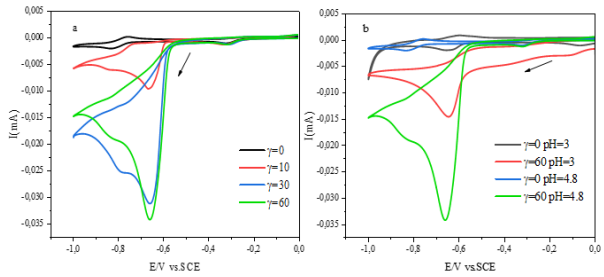


Figure 11. (a): Nitrite Electroreduction in the presence of 1×10^{-4} M POM-Fe in acetate buffer at pH 4.8. (b): Comparison of nitrite Electroreduction at pH 4.8 and pH 3 medium.The scan rate υ = $2mV.s^{-1}$.

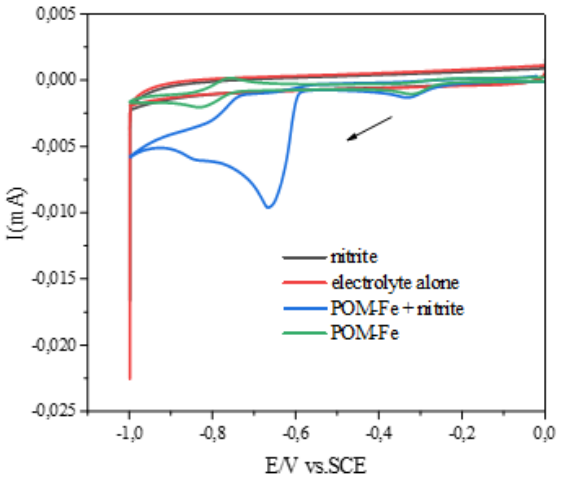


Figure 12. Comparative cyclic voltammetry of nitrite, electrolyte alone, POM-Fe, and POM-Fe with nitrite.

During electrolysis at −0.40 V, the solution gradually developed a pale red coloration, which may be associated with the formation of a nitrosyl-type intermediate coordinated to the ferrous center (POM–Fe–NO). This observation is consistent with the results reported by Tóth *et al.* (1989), who attributed similar coloration to the formation of an Fe–NO nitrosyl complex following the one-electron reduction of Fe^{3+} to Fe^{2+}.

In contrast, when electrolysis was continued at −0.90 V, the solution turned deep blue, a color typical of strongly reduced tungstate heteropolyanions (Tóth *et al.* 1989), suggesting significant electron accumulation within the polyoxometalate framework. Analysis of the solution immediately after the two electrolysis steps using Nessler's reagent suggested the formation of ammonium species, as indicated by the appearance of an intense yellow coloration (**Figure 13**).



Figure 13. Nessler's reagent test of the electrolyzed solution after successive electrolysis at −0.4 and −0.9 V vs. SCE, confirming the presence of ammonium ions.

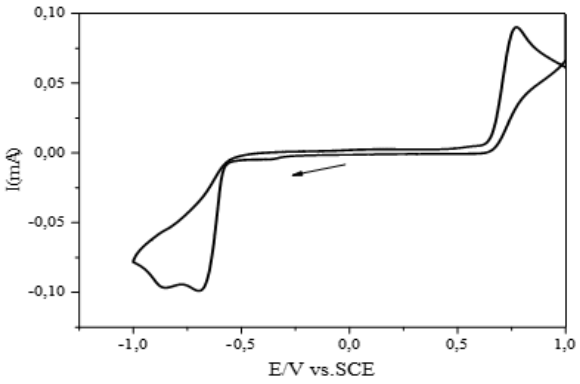


Figure 14. Cyclic voltammetry after two-step electrolysis (−400 and −900 mV vs. SCE), highlighting the $Fe^{2+} \rightarrow Fe^{3+}$ anodic oxidation wave at +0.70 V.

These results suggest that ammonium formation may occur at −0.90 V following the deeper reduction of the POM–Fe–NO nitrosyl intermediate. This process is likely facilitated by electrons stored on the tungsten centers of the reduced POM–Fe, which may act as a multielectron reservoir, contributing to the reduction of the Fe–NO species toward NH_4^+. In addition, after the two electrolysis steps, a new anodic wave appears at approximately +0.70 V, which can

be assigned to the $Fe^{2+} \rightarrow Fe^{3+}$ oxidation process, supporting the involvement of the iron center in the redox cycle (**Figure 14**).

By contrast, when a single electrolysis was directly applied at −0.90 V without a preliminary step at −0.40 V, no coloration was observed after addition of Nessler's reagent, suggesting the absence of detectable NH_4^+ formation under these conditions (**Figure 13**). This observation indicates that prior formation of the POM–Fe–NO nitrosyl intermediate may play an important role in the electrocatalytic reduction of nitrite. In this context, the initial one-electron reduction of the iron center ($Fe^{3+} \rightarrow Fe^{2+}$) may enable nitrite activation through the formation of an Fe–NO type intermediate, which could subsequently undergo further reduction processes driven by electrons supplied by the reduced polyoxometalate framework.

The proposed mechanistic sequence can be summarized as follows:

Step 1. Electrolysis around −0.40 V: formation of the nitrosyl intermediate

Step 2. Electrolysis at −0.90V: deep multielectron reduction and NH_4^+ formation

Overall, the electrocatalytic reduction of nitrite by POM–Fe is proposed to proceed through a two-step mechanism: (1) nitrite activation via possible nitrosyl intermediate formation following iron-center reduction, and (2) further multielectron reduction of this intermediate mediated by the tungsten centers of the polyoxometalate framework, potentially leading to ammonium formation.

To evaluate the reproducibility of the electrocatalytic measurements, all experiments were performed in triplicate under identical experimental conditions. The individual measurements, together with the corresponding mean values and standard deviations (SD), are summarized in Table 4. The catalytic efficiency (CAT) values are reported as mean ± SD, and the error bars shown in **Figure 15** represent the standard deviation of three independent measurements. Statistical analysis was performed using a two-way analysis of variance (ANOVA) (Table 5) to assess the effects of pH and nitrite concentration on the catalytic performance of POM–Fe. The results revealed that both pH ($F = 119199.73$, $p < 0.0001$) and nitrite concentration ($F = 79662.53$, $p < 0.0001$) significantly affect the catalytic efficiency. Moreover, a significant interaction between these two factors was observed ($F = 9760.89$, $p < 0.0001$), indicating that the effect of nitrite concentration depends strongly on the solution pH. The relatively small standard deviation values obtained for all measurements demonstrate the excellent reproducibility and reliability of the electrochemical experiments. These results further indicate that the catalytic efficiency of POM–Fe is strongly influenced by both pH and nitrite concentration, with the highest catalytic activity observed at pH 4.8 and elevated nitrite concentrations.

Table 4. Mean catalytic activity (CAT%) ± standard deviation (n = 3) under different pH and nitrite concentrations.

pH	$[NO_2^-]$ (M)	CAT (%)
3	1×10^{-3}	72.72 ± 2.51
3	3×10^{-3}	608.53 ± 4.33
3	6×10^{-3}	633.71 ± 3.45
4.8	1×10^{-3}	371.93 ± 3.09
4.8	3×10^{-3}	1431.86 ± 4.79
4.8	6×10^{-3}	1571.05 ± 6.11

Table 5. Statistical significance analysis (ANOVA) of catalytic activity (CAT%) at different experimental conditions.

Source	df	F-value	p-value
pH	1	119199.73	<0.0001
$[NO_2^-]$	2	79662.53	<0.0001
pH × Nitrite concentration	2	9760.89	<0.0001

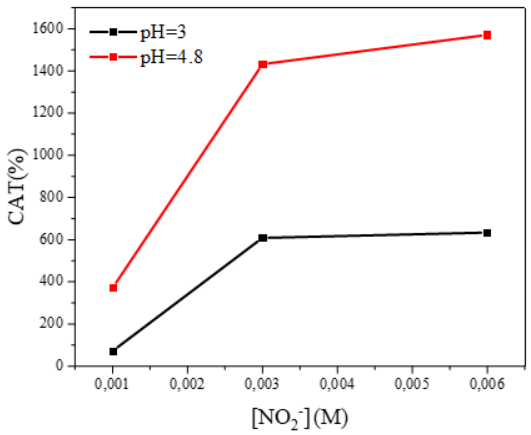


Figure 15. Variation of catalytic efficiency (%) as a function of nitrite concentration (mean ± SD, n = 3).

4. Conclusions

In this work, an iron-rich sandwich-type polyoxometalate, $K_4Na_7[(\alpha\text{-}SiFe_3W_9(OH)_3O_{34})_2(OH)_3]\cdot56H_2O$ (POM–Fe), was synthesized through a controlled buffered strategy at pH 4.8 and characterized using complementary structural, spectroscopic, thermal, magnetic, and electrochemical techniques. Powder X-ray diffraction, together with single-crystal analysis, indicated that the obtained compound is consistent with the previously reported Anderson-type sandwich architecture, supporting the reproducibility of the synthetic approach.

Electrochemical investigations showed that POM–Fe exhibits notable electrocatalytic activity toward nitrite reduction. The catalytic performance is strongly pH-dependent, highlighting the role of nitrite speciation and

stability in the reaction medium. Controlled electrolysis experiments, combined with qualitative detection of ammonium, suggest that nitrite reduction may proceed through a two-step pathway involving the formation of an Fe–NO type intermediate, followed by further multielectron reduction processes facilitated by the polyoxotungstate framework acting as an electron reservoir.

The reproducibility of the electrochemical measurements was assessed through triplicate experiments. Statistical analysis, including standard deviation calculations and two-way ANOVA, indicated that pH and nitrite concentration influence the catalytic efficiency of POM–Fe, with higher catalytic activity observed at pH 4.8 and elevated nitrite concentrations. From an environmental perspective, these findings are relevant to the development of catalytic systems for the mitigation of nitrite pollution in aqueous media and for the transformation of nitrogen-containing species under mild electrochemical conditions. The novelty of the present work lies in the reproducible preparation of the Fe_6 sandwich-type polyoxometalate under controlled buffered conditions at pH 4.8 and in its first electrocatalytic investigation toward nitrite reduction in homogeneous solution. The qualitative detection of ammonium following electrolysis further supports the potential of this iron-rich POM for nitrite conversion. Overall, this study provides preliminary insight into the electrocatalytic behavior of iron-substituted sandwich polyoxometalates and contributes to the exploration of POM-based systems for environmentally relevant nitrogen conversion reactions.

References

Anderson, T. M., Neiwert, W. A., Hardcastle, K. I., Hill, C. L. 2004. Multi-Iron Silicotungstates: Synthesis, Characterization, and Stability Studies of Polyoxometalate Dimers. Inorganic Chemistry, 43, 7353-7358. https://doi.org/10.1021/ic049517s.

Anderson, T. M., Cao, R., Neiwert, W. A., Hardcastle, K. I., Hill, C. L., Amman, M., Keita, B., Nadjo, L. 2005. Structural and Electrochemical Studies of Dimerization and Rotational Isomerization in Multi-Iron Silicotungstates. European Journal of Inorganic Chemistry, 1770–1775. https://doi.org/10.1002/ejic.200401061.

Bao, W., Feng, C., Wang, C., Liu, D., Fan, X., Liang, P. 2025. Polyoxometalates in Electrochemical Energy Storage: Recent Advances and Perspectives. International Journal of Molecular Sciences, 26, 10267. https://doi.org/10.3390/ijms262110267.

Belhouari, A., Keita, B., Nadjo, L., Contant, R. 1998. Efficient conversion of NO into N2O by selected electroreduced heteropolyanions. New Journal of Chemistry, 22, 83-86. https://doi.org/10.1039/A708728D.

Bi, L. H., Kortz, U., Nellutla, S., Stowe, A. C., van Tol, J., Dalal, N. S., Keita, B., Nadjo, L. 2005. Structure, Electrochemistry, and Magnetism of the Iron(III)-Substituted Keggin Dimer, $[Fe_6(OH)_3(A\text{-}\alpha\text{-}GeW_9O_{34}(OH)_3)_2]^{11-}$. Inorganic Chemistry, 44, 896-903. https://doi.org/10.1021/ic048713w.

Cherevan, A. S., Nandan, S. P., Roger, I., Liu, R., Streb, C., Eder, D. 2020, Polyoxometalates on Functional Substrates : Concepts, Synergies, and Future Perspectives. Advanced Science, 7, 1903511. https://doi.org/10.1002/advs.201903511.

Fewtrell, L. 2004. Drinking-Water Nitrate, Methemoglobinemia, and Global Burden of Disease : A Discussion. Environ Health Perspect, 112, 1371–1374. https://doi.org/10.1289/ehp.7216.

Genders, D. J., Hartsough, D., Hobbs, D. T. 1996. Electrochemical reduction of nitrates and nitrites in alkaline nuclear waste solutions. Journal of Applied Electrochemistry, 26, 1–9. https://doi.org/10.1007/BF00248182.

Gusmão, F. M. B., Mladenović, D., Radinović, K., Santos, D. M. F., Šljukić, B. 2022. Polyoxometalates as Electrocatalysts for Electrochemical Energy Conversion and Storage. Energies, 15, 9021. https://doi.org/10.3390/en15239021.

Keita, B., Girard, F., Nadjo, L., Contant, R., Belghiche, R., Abbessi, M. 2001. Cyclic voltammetric evidence of facilitation of the reduction ofnitrite by the presence of molybdenum in Fe- or Cu-substituted heteropolytungstates. Journal of Electroanalytical Chemistry, 508, 70–80. https://doi.org/10.1016/S0022-0728(01)00516-2.

Keita, B., Mbomekalle, M. I., Nadjo, L. 2003. Redox behaviours and electrocatalytic properties of copper within Dawson structure-derived sandwich heteropolyanions $[Cu_4(H_2O)_2(X_2W_{15}O_{56})_2]^{16-}$ (X= P or As). Electrochemistry Communications, 5, 830-837. https://doi.org/10.1016/j.elecom.2003.07.005.

Li, H. L., Robertson, D. H., Chambers, J. Q., Hobbs, D. T. 1988. Electrochemical Reduction of Nitrate and Nitrite in Concentrated Sodium Hydroxide at Platinum and Nickel Electrodes. Journal of The Electrochemical Society, 135, 1154. https://doi.org/10.1149/1.2095900.

Li, K., Liu, T., Ying, J., Tian, A., Wang, X. 2024. Recent research progress on polyoxometalate-based electrocatalysts in energy generation. Journal of Materials Chemistry A, 12, 13576-13604. https://doi.org/10.1039/D4TA01636J.

Li, M. X., Zhang, Y., Zhu, Z. M., Su, F., Zhang, L. C., Sang, X. J. 2020, Synthesis, characterization and electrocatalytic properties of two new open Wells-Dawson-type tungstosilicates. Journal of Coordination Chemistry. 73, 2437. https://doi.org/10.1080/00958972.2020.1811857.

McCormac, T., Fabre, B., Bidan, G. 1997. Part II. Role of pH and the transition metal for the electrocatalytic reduction of nitrite with transition metal substituted Dawson type heteropolyanions. Journal of Electroanalytical Chemistry, 427,155–159. https://doi.org/10.1016/S0022 0728(96)04991-1.

Moore, J. M., Fout, A. R. 2025. Tetrapodal iron complexes invoke observable intermediates in nitrate and nitrite reduction. Chemical Science, 16, 840-845. https://doi.org/10.1039/D4SC06570K.

Nellutla, S., van Tol, J., Dalal, N. S., Bi, L. H., Kortz, U., Keita, B., Nadjo, L., Khitrov, G. A., Marshall, A. G. 2005. Magnetism, Electron Paramagnetic Resonance, Electrochemistry, and Mass Spectrometry of the Pentacopper(II)-Substituted Tungstosilicate $[Cu_5(OH)_4(H_2O)_2(\alpha\text{-}SiW_9O_{33})_2]^{10-}$, A Model Five-Spin Frustrated Cluster. Inorganic Chemistry, 44, 9795-9806. https://doi.org/10.1021/ic0512633.

Ni, L., Hussain, F., Spingler, B., Weyeneth, S., Patzke, G. R. 2011. Lanthanoid-Containing Open Wells-Dawson Silicotungstates: Synthesis, Crystal Structures, and Properties. Inorganic Chemistry, 50, 4944-4955. https://doi.org/10.1021/ic2001943

Ni, L., Spingler, B., Weyeneth, S., Patzke, G. R. 2013. Trilacunary Keggin-Type POMs as Versatile Building Blocks for Lanthanoid Silicotungstates. European Journal of Inorganic Chemistry, 1681- 1692. https: //doi.org/10.1002/ejic.201201186.

Picetti, R., Deeney, M., Pastorino, S., Miller, M. R., Shah, A., Leon, D. A., Dangour, A. D., Green, S. 2022. Nitrate and nitrite contamination in drinking water and cancer risk: A systematic review with meta-analysis. Environmental Research, 210, 112988. https://doi.org/10.1016/j.envres.2022.112988.

Ruhlmann, L., Genet, G. 2004. Wells–Dawson-derived tetrameric complexes $\{K_{28}H_8[P_2W_{15}Ti_3O_{60.5}]_4\}$ electrochemical behaviour and electrocatalytic reduction of nitrite and of nitric oxide. Journal of Electroanalytical Chemistry, 568, 315–321. https://doi.org/10.1016/j.jelechem.2004.02.020.

Ruhlmann, L., Canny, J., Contant, R., Thouvenot, R. 2002. Di- and Tricobalt Dawson Sandwich Complexes: Synthesis, Spectroscopic Characterization, and Electrochemical Behavior of $Na_{18}[(NaOH_2)_2Co_2(P_2W_{15}O_{56})_2]$ and $Na_{17}[(NaOH_2)Co_3(H_2O)(P_2W_{15}O_{56})_2]$. Inorganic Chemistry, 41, 3811. https://doi.org/10.1021/ic020146u.

Ruhlmann, L., Costa-Coquelard, C., Canny, J., Thouvenot, R. 2007. Electrochemical and electrocatalytical investigations on the trimanganese sandwich complex $[NaMn_3(H_2O)_2(P_2W_{15}O_{56})_2]^{17-}$. Journal of Electroanalytical Chemistry, 603, 260-268. https://doi.org/10.1016/ j.jelechem.2007.02.017.

Tézé, A., Hervé, G. 1990. Inorganic Syntheses. Wiley, 27, 85

Toth, J. E., Anson, F. C. 1989. Electrocatalytic Reduction of Nitrite and Nitric Oxide to Ammonia with Iron-Substituted Polyoxotungstates. Journal of the American Chemical Society, 111, 7, 2444–2451. https://doi.org/10.1021/ja00189a012.

Wang, Y., Fang, G., Ordomsky, V. V., Khodakov, A. Y. 2025. Polyoxometalate photocatalysts : solar-driven activation of small molecules for energy conversion and greenhouse gas valorization. Chemical Communications, 61, 10630–10642. https://doi.org/10.1039/D5CC01494H.

Ward, M. H., Jones, R. R., Brender, J. D., de Kok, T. M., Weyer, P. J., Nolan, B. T., Villanueva, C. M., van Breda, S. G. 2018. Drinking Water Nitrate and Human Health: An Updated Review. International Journal of Environmental Research and Public Health, 15, 1557. https://doi.org/10.3390/ijerph15071557.

Zhou, Y., Bihl, F., Bonnefont, A., Boudon, C., Ruhlmann, L., Badets, V. 2022. Selectivity and efficiency of nitrite electroreduction catalyzed by a series of Keggin polyoxometalates. Journal of Catalysis, 405, 212–223. https://doi.org/10.1016/j.jcat.2021.11.037.

Zhu, G., Geletii, Y. V., Zhao, C., Musaev, D. G., Song, J., Hill, C. L. 2012. A dodecanuclear Zn cluster sandwiched by polyoxometalate ligands. Dalton Transactions, 41. https://doi: 10.1039/c2dt30733b.

Zonoz, F. M., Aliabadi, F. 2016. A new sandwich-type polyoxometalates containing mixed transition metals, $[Cd_2Zn_2(H_2O)_2(P_2W_{15}O_{56})_2]^{16-}$: Syntheses, spectrochemical characterization and its electrocatalytical activity comparison with $[M_4(H_2O)_2(P_2W_{15}O_{56})_2]^{16-}$ (M = Cd^{2+} and Zn^{2+}) and $[P_2W_{15}O_{56}]^{12-}$. Inorganica Chimica Acta, 444, 87. https://doi.org/10.1016/j.ica.2016.01.030.